Food and Chemical Toxicology 127 (2019) 1–10

Contents lists available at ScienceDirect

Food and Chemical Toxicology

journal homepage: www.elsevier.com/locate/foodchemtox

Low-dose exposure to triclosan disrupted osteogenic differentiation of mouse embryonic stem cells via BMP/ERK/Smad/Runx-2 signalling pathway

Wei Cheng[a], Shoufei Yang[a], Fan Liang[a], Wei Wang[a], Ren Zhou[b], Yan Li[a], Yan Feng[a], Yan Wang[a,b,c,*]

[a] College of Public Health, School of Medicine, Shanghai Jiaotong University, Shanghai, 200025, PR China
[b] The Ninth People's Hospital of Shanghai Jiao Tong University School of Medicine, Shanghai, 200011, PR China
[c] MOE-Shanghai Key Laboratory of Children's Environmental Health, Shanghai, 200092, PR China

ARTICLE INFO

Keywords:
Triclosan
Skeletal development
Low dose effect
Embryonic stem cell
Runx-2

ABSTRACT

Triclosan (TCS) has been used widely in personal care products for its broad-spectrum antimicrobial activity. The detection of TCS in the umbilical cord sera, amniotic fluid, and placenta, has raised concerns about the risk to foetal development. In the current study, the embryonic stem cells test (EST) were utilized primarily for the evaluation of the adverse effects of TCS on cardiogenesis and osteogenesis *in vitro*. TCS was predicted to be weakly embryotoxic in cardiogenesis and strongly embryotoxic in osteogenesis. The 50% inhibition value of osteogenic differentiation was 110 times lower than that of cardiac differentiation, which suggested that the development of the skeletal system was more sensitive to TCS-induced disruption. The mechanism through which TCS exerted toxicity on osteogenesis was studied further. Decreased calcification in ESC-derived osteoblasts was observed after exposure to TCS at a low dose, equal to the human internal exposure level. TCS was observed to specifically target ERK activation, rather than JNK or p38. Further, the downregulation of p-Smad-1, together with strong inhibition on Runx-2 and Bglap-2 expression, was observed via BMP/ERK/Smad signalling when cells were exposed to TCS. The change in Runx-2 induced by a low-dose TCS highlighted a specific target for exploring its adverse effect on skeletal development.

1. Introduction

Triclosan (TCS), an antimicrobial ingredient, has been used widely in personal care products for its broad-spectrum antimicrobial activity. It is used in toothpaste, soaps, and antiperspirants, as well as in consumer products such as toys and clothes (Rodricks et al., 2010). TCS has been identified as an endocrine disruptor, which targets the oestrogen receptor or androgen receptor and functions antagonistically (Farmer et al., 2018). It also affects thyroxine homeostasis in both maternal animals and their offspring (Hua et al., 2017; Jackson et al., 2018). TCS is detectable in various biological samples, including urine, serum, the placenta, amniotic fluid, and cord blood, at concentrations of 0.01–38 ng/ml (James et al., 2010; Philippat et al., 2013; Scinicariello and Buser, 2016; Shekhar et al., 2017; Wang et al., 2018). In previous studies, the association between TCS and its adverse outcomes has been investigated. The target organs were reported to be the liver, spleen, brain, heart, reproductive system, and the immune system (Ibtisham et al., 2016; Johnson et al., 2016; Scinicariello and Buser, 2016).

Compared with other well-identified target organs (Haggard et al., 2016; Pernoncini et al., 2018; Wang et al., 2017b), higher concentrations of up to 7 ng/ml TCS can be detected in the placenta, cord blood, and amniotic fluid, which indicate a higher risk of adverse effects on the embryo *in utero* directly (Axelstad et al., 2013; James et al., 2010; Shekhar et al., 2017; Yao et al., 2018).

Research conducted to date has improved the understanding of the developmental toxicity induced by TCS. When zebrafish (*Danio rerio*) are exposed to a non-cytotoxic dose of TCS, abnormal lipid droplets accumulate in the yolk sac. This provided preliminary evidence of a malformation potential (Chen et al., 2015b). As the embryos develop, the administration of more than 40 μg/L TCS induces a delay in hatching and pericardial oedema in the developing heart, and alterations in the cardiac structure and output (Ho et al., 2016; Saley et al.,

* Corresponding author. No. 639 Zhizaoju Road, Shanghai, 200011, PR China.
E-mail addresses: mishua_@hotmail.com (W. Cheng), yangshou_fei@163.com (S. Yang), sharuru@yeah.net (F. Liang), 1490432268@qq.com (W. Wang), 318281114@qq.com (R. Zhou), liyan86414048@126.com (Y. Li), fy_575@sjtu.edu.cn (Y. Feng), wangyan@shsmu.edu.cn (Y. Wang).

https://doi.org/10.1016/j.fct.2019.02.038
Received 8 November 2018; Received in revised form 20 February 2019; Accepted 25 February 2019
Available online 02 March 2019
0278-6915/

2016). In addition, it affects pigmentation in the eyes and body, causes discoloration in the liver, produces significant spinal deformities and abnormal length, and induces lethality to embryos or causes undersized new-born zebrafish without inducing any significant effect on the expression of pluripotency markers, such as *Oct-4*, *Sox-2*, or *Nanog*, in the embryo stage (Saley et al., 2016). In addition, irregular ossification of the skull has been recorded in the offspring of TCS-exposed pregnant CD-1 mice. Significant decreases in the ossification of the forepaw and hind paw phalanges per foetus per litter have been observed (Argus Research Laboratories Protocol 403–010, 1992). Despite the existence of abnormal skeletal phenotypes, no study has yet been conducted to investigate the possible molecular mechanism of TCS-induced developmental skeletal toxicity.

Embryonic stem cells (ESCs) are characterized as pluripotent and self-renewable; they can be induced to differentiate into various tissue-specific cell types, such as cardiomyocytes, neural progenitor cells, hepatocytes, or osteoblasts. It is therefore possible to mimic embryo development *in vitro*, and abnormalities can be detected following exposure to xenobiotics, and these are closely related to phenotypes that have been observed *in vivo* (Cheng et al., 2013; Kamelia et al., 2017; Shi et al., 2017; Yin et al., 2018). Based on this property, a successful example is the embryonic stem cell test (EST), an alternative method validated by the European Union Reference Laboratory for alternatives to animal testing (EURL-ECVAM) for the prediction of developmental toxicity (Seiler and Spielmann, 2011). By utilizing mouse ESCs and ESC-derived cardiomyocytes, the tested chemicals can be predicted as non-embryotoxic, weakly embryotoxic, or strongly embryotoxic via three predictive formulas, leading to a total accuracy of more than 80% after many modifications for refinement (Cheng et al., 2016b; Dimopoulou et al., 2018; Seiler and Spielmann, 2011; Yu et al., 2015).

In addition, during embryo development, bone morphogenetic protein (BMP) signalling plays a critical role in the development of both the heart and bone through the activation of a cascade of downstream signals or tissue-specific transcription factors (Jain et al., 2015; Qi et al., 2007; Wu et al., 2016). Thus, following the BMP-Smad signalling pathway would help to identify the target genes of TCS, as TCS-induced developmental osteogenic toxicity and its mechanisms have not been well investigated.

Therefore, in the current study, to determine the embryotoxicity of TCS to cardiomyocytes and osteoblasts, we used a dual-organ test system consisting of cardiomyocytes and osteoblasts derived from ESCs (termed ESTcardio and ESTosteo, respectively) proposed to identify sensitive target organs, and focused on the effects on the BMP-Smad signalling pathway observed at non-cytotoxic concentrations.

2. Materials and methods

2.1. Cell culture

The ESC line R1 (ATCC: SCRC-1011), which was commercially purchased, was cultivated on gelatin-coated culture dishes. ESC medium consisted of KnockOut Dulbecco's Modified Eagle's medium (KO DMEM, Gibco, USA), 10% foetal calf serum (Gibco, USA), 0.1 mM beta-mercaptoethanol (Gibco, USA), 2 mM L-glutamine (Gibco, USA), 0.1 mM nonessential amino acids (Gibco, USA), and 1000 U/ml leukaemia inhibitory factor (LIF, Millipore, USA).

To induce cardiac differentiation, ESCs were digested into single cells with 0.25% Trypsin/EDTA (Gibco, USA), and a total of 800 R1 ESC cells were cultured in 20 μl hanging drops to generate embryoid bodies (EBs) in DMEM with 15% foetal calf serum (Gibco, USA). Subsequently, 40 EBs were placed onto each culture dish cover (Corning, USA) for each concentration of TCS (purity 99%, Sigma-Aldrich, USA) for 3 days, and then EBs were cultivated in suspension in a non-adhesive bacterial culture dish (Alpha, China) for each concentration of TCS (CAS: 3380-34-5, Sigma, USA) for 2 days. On Day 5, EBs were plated into each well of a 96-well plate (Corning, USA) with TCS until Day 10. The medium was changed every 2 days. On Day 10 of the differentiation process, the contractile cardiomyocytes were examined microscopically. The dosages used in cardiac differentiation ranged from 500 to 40,000 ng/ml.

To induce osteogenic differentiation, the first steps were similar to those of cardiac differentiation. On Day 5, EBs were plated into each well of a 24-well plate (Corning, USA) in DMEM with 15% FBS, 0.1 mM β-mercaptoethanol (Gibco, USA), 50 μg/ml ascorbic acid (Sigma-Aldrich, USA), 10 mM β-glycerophosphate (Sigma-Aldrich, USA) and 5×10^{-8} M 1,25-dihydroxyvitamin D3 (Sigma-Aldrich, USA) to induce osteoblast differentiation. The culture medium supplemented with varying concentrations of TCS was changed every 3 days until Day 30. The dosages used in osteogenic differentiation ranged from 3 to 2500 ng/ml. In addition, 2.5×10^{-11} M tamoxifen (TX) (purity 99%, J&K, Germany) and 1×10^{-11} M oestradiol (E2) (purity 99%, J&K, Germany) were selected as the negative- and positive-control, respectively, and were added into the medium from Day 25 to Day 30.

In addition, NIH3T3 fibroblasts (ATCC CRL-1658) were cultivated in DMEM with 10% FBS.

2.2. Cell viability assay

Alamar blue reagent (ThermoFisher, USA) was used to determine cellular viability in accordance with the manufacturer's instructions. In total, 500 R1 ESCs and 1000 NIH3T3 cells were seeded in separate wells of a 96-well tissue culture plate, and were exposed to varying concentrations of TCS, as well as 5-fluorouracil (5-FU, CAS: 51-21-8, Sigma, USA) and penicillin G (PG, CAS: 69-57-8, Wako, Japan). The medium with TCS was changed every 2 days. On Day 5 of cultivation, the cytotoxic effects of chemicals were determined by using a TriStar LB 941 Multimode microplate reader (Berthold, Germany), and the fluorescence was measured at excitation and emission wavelengths of 550 nm and 590 nm, respectively. The concentrations of 50% inhibition of cellular proliferation (IC_{50}) of 3T3 and ESC were then calculated. In addition, the cytotoxic effects of the exposed chemicals during the osteogenic differentiation of ESC were determined.

2.3. Immunofluorescence staining assay

ESC-derived cardiomyocytes were fixed and stained as described in a previous study (Cheng et al., 2016a). The primary antibodies were mouse anti-alpha myosin heavy chain (α-MHC) (Abcam, USA), and rabbit anti-Nkx-2.5 (Abcam, USA); the secondary antibodies were Alexa Fluor® 565-labelled goat anti-mouse IgG (ThermoFisher, USA) and Alexa Fluor® 488-labelled donkey anti-rabbit IgG (ThermoFisher, USA). The cell nuclei were stained with 4,6-diamidino-2-phenylindole (DAPI) (Beyotime, China), sealed with coverslips and an anti-fade reagent (ThermoFisher, USA), and then observed by using a fluorescence microscope.

2.4. Counting of positive beating rate in ESC-derived cardiomyocytes

ESC-derived cardiomyocytes were harvested on Day 10, and the beating rate of each exposed group (40 EBs per group) was recorded. The differentiated cells were considered as positive contractile cardiomyocytes if at least one beating foci was observed in each well of a 96-well plate; the positive beating rate was normalized to that of the control group.

2.5. Alizarin red S (ARS) staining

ARS is a calcium-specific chelating agent that accumulates in the cellular matrix in the presence of calcium. The ESC-derived osteoblasts were fixed, washed with 0.9% NaCl, and then incubated for 20 min at room temperature in a solution containing 1% of alizarin red S (purity 99%, J&K, China) at pH 4.2. The positive staining results were observed microscopically.

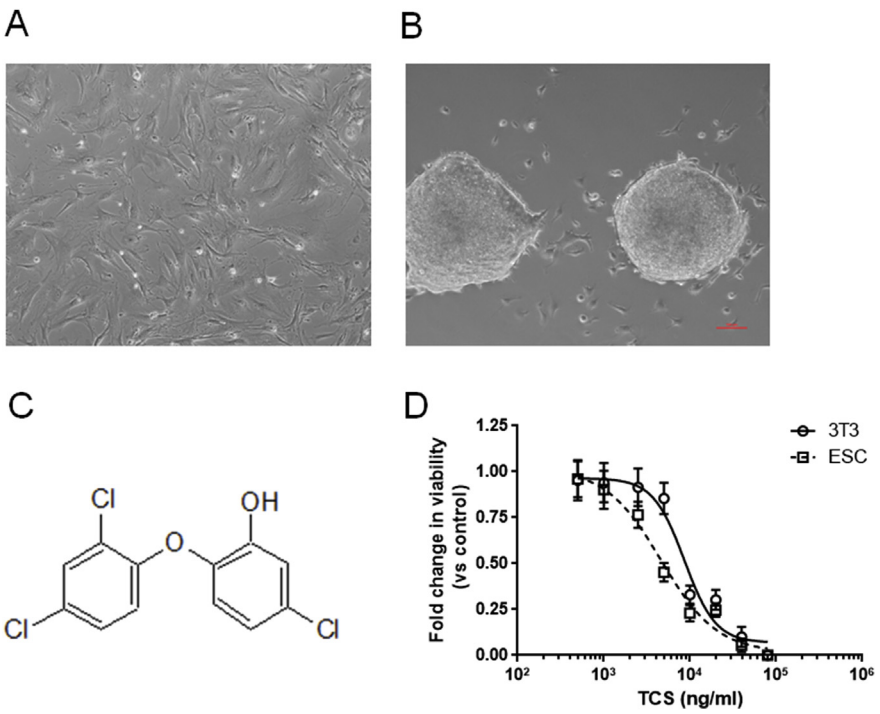

Fig. 1. Cytotoxicity of TCS on NIH3T3 fibroblasts and ESC. (A) and (B) Microscopy images of NIH3T3 fibroblasts and ESCs, respectively. Scale bar = 100 μm. (C) Chemical structure of TCS. (D) Dose-response curve of cytotoxicity when cells were exposed to different concentrations of TCS. The data from three independent experiments performed in triplicate are presented as the mean ± SEM.

2.6. Determination of calcium content

The ESC-derived osteoblasts were rinsed with PBS twice to remove the chemicals in the medium and then lysed in radioimmunoprecipitation (RIPA) buffer. The protein concentrations in lysates were determined by using a BCA assay kit (Beyotime, China). To quantify the calcium concentration, an arsenazo III assay (J&K, Germany) was performed by addition into the lysates and measurement of the absorbance at 650 nm on a microplate spectrophotometer (BioTek, USA), as described previously (zur Nieden et al., 2015). The data were normalized to the total protein content and compared with the control group.

2.7. Determination of tartrate-resistant acid phosphatase (TRAP) activity

The TRAP activity of ESC-derived osteoblasts was measured by using a commercial kit (Beyotime, China) in accordance with the manufacturer's instructions. The data were normalized to the value acquired for the control group.

2.8. Determination of alkaline phosphatase (AKP) activity

The AKP activity in the suspension medium of ESC-derived osteoblasts was measured by using a commercial kit (Beyotime, China) in accordance with the manufacturer's instruction. The data were normalized to the protein content determined by a BCA assay for each group.

2.9. RNA extraction and quantitative real-time PCR analysis

ESC-derived cardiomyocytes were harvested on Day 10, and ESC-derived osteoblasts were harvested on Day 30. The total RNA was extracted by using the Trizol reagent (Invitrogen, USA) in accordance with the manufacturer's instructions. The concentration of total RNA was quantified by the absorbance at 260 nm by using a NanoDrop spectrophotometer (ThermoFisher, USA). Reverse transcription was performed with a PrimeScript® RT reagent Kit (Takara, Japan), and real-time PCR was performed in triplicate with a SYBR® Premix Ex Taq™ II RT-PCR Kit (Takara, Japan) on a Roche LightCycler® 480 System (Roche, Switzerland). Relative gene expression was calculated by the $-2^{\triangle\triangle Ct}$ method against the internal reference gene of glyceraldehyde-3-phosphate dehydrogenase (GAPDH). The quantitative PCR amplification was performed using the following conditions: 1 cycle of 95 °C, 30 s; followed by 40 cycles of 95 °C, 5 s and 60 °C, 30 s. An additional procedure of 95 °C, 15 s, followed by 60 °C, 60 s and 95 °C, 15 s was used for dissociation curve acquisition. The primer sequences are found in Table S1.

Accordingly, the values for 50% inhibition of differentiation (ID_{50}) from ESCs into cardiomyocytes ($ID_{50\ cardio}$) and osteoblasts ($ID_{50\ osteo}$) were calculated.

2.10. Western blotting

Western blotting was performed as described previously (Cheng et al., 2016a). The cells were lysed with RIPA buffer. The proteins concentrations were detected by using a BCA protein assay kit (Beyotime, China). The primary antibodies used were: BMP-2 (Santa Cruz, USA), Smad-1 (Santa Cruz, USA), p-Smad-1 (Beyotime, China), Runx-2 (Santa Cruz, USA), Bglap-2 (Santa Cruz, USA), ERK1/2, p-ERK1/2, JNK, p-JNK, p38, p-p38 (Beyotime, China), and β-actin (Cell Signalling Technology, USA). The cells were cultivated with secondary antibodies, and an enhanced chemiluminescence luminol reagent (Millipore, USA) was used to reveal the protein bands. The densities of protein bands in each sample were calculated by using Quantity One software (BioRad, USA).

2.11. Statistical analysis

Three independent experiments were performed in triplicate. The data are expressed as the mean ± standard error (SEM) and presented to four significant digits. The data were subjected to one-way analysis of variance (ANOVA) applied by using SPSS Version 19 for Windows (SPSS Inc., Chicago, USA), with the LSD *post hoc* test used for multiple group comparisons. A significant difference was indicated by $p < 0.05$.

Table 1
Summary of values for embryotoxicity prediction of TCS based on cardiac and osteogenic differentiation of ESC.

	Values of 50% inhibition (μg/ml)			Prediction formula			Prediction result
		Mean	SEM	I	II	III	
Viability (IC_{50})	3T3	8.290	1.022	–	–	–	–
	ESC	3.670	0.8617	–	–	–	–
Cardiac differentiation ($ID_{50\ cardio}$)	Beating	14.38	3.071	−3.961	−0.6511	−4.969	weakly-embryotoxic
	Myh6	14.77	1.337	−3.711	−0.5554	−5.040	weakly-embryotoxic
	Myl4	35.41	4.045	9.502	4.506	−8.774	non-embryotoxic
Osteogenic differentiation ($ID_{50\ osteo}$)	Ca2+	0.3142	0.1261	−12.97	−4.101	−2.424	strongly-embryotoxic
	Bglap-2	0.1091	0.08194	−13.10	−4.151	−2.387	strongly-embryotoxic
	SPARC	0.1892	0.09022	−13.05	−4.132	−2.402	strongly-embryotoxic

3. Results

3.1. The cytotoxicity of TCS on NIH3T3 cells and ESCs

The NIH3T3 cells differed from ESC morphologically (Fig. 1A and B).

In the EST, the NIH3T3 cells were used to represent the chemical-induced effect on “adult” tissue, whereas ESCs were used to mirror the chemical-induced adverse effects on embryonic development *in vitro*.

TCS induced cytotoxicity in both NIH3T3 cells and ESCs in a dose-dependent manner (Fig. 1D). For $IC_{50\ 3T3}$ and $IC_{50\ ESC}$, the IC_{50} values were calculated and are listed in Table 1. In addition, according to the dose-response curve of the tested chemicals (Fig. S1), the $IC_{50\ 3T3}$ values of 5-FU and PG were calculated and listed accordingly (Table S2).

3.2. TCS disrupted cardiac differentiation

As shown in Fig. 2A, α-MHC-positive and Nkx-2.5-positive cells were located in and surrounded the EB centre, which was in accordance with the beating area observed by using a microscope (see Supplementary Data). It suggested the successful differentiation of ESCs to cardiomyocytes. As shown in Fig. 2B, the positive beating rate of ESC-derived cardiomyocytes decreased in a dose-dependent manner when ESC-derived cardiomyocytes were exposed to varying concentrations of TCS. A drastic decrease in beating rate was observed at dosages of 2500 ng/ml. The mRNA expression of *Myh-6* and *Myl-4*, which encode the cardiac structural proteins α-MHC and myosin light chain (MLC1a), decreased in a dose-dependent manner following TCS exposure, as shown in Fig. 2C. Consequently, the ID_{50} values of cardiac differentiation ($ID_{50\ cardio}$) were calculated based on the beating rate as well as the mRNA expression of *Myh-6* and *Myl-4*, respectively (Table 1).

Similarly, the $ID_{50\ cardio}$ values of 5-FU and PG were calculated (Table S2).

3.3. TCS disrupted osteogenic differentiation

The ARS was used to determine the mineral nodules in ESC-derived osteoblasts. As shown in Fig. 3A, a large number of positive-stained foci, in the form of red-stained areas with low optic density, could be observed, together with the positive expression of osteogenic-specific markers, such as *Bglap-2* and secreted protein acidic and rich in cysteine (*SPARC*) (Fig. 3C). This was suggestive of the successful differentiation of ESC toward osteoblasts. When cells were exposed to varying concentrations of TCS, a dose-dependent decrease in the calcium concentration and the mRNA expression of *Bglap-2* and *SPARC* were observed. Based on these endpoints, the ID_{50} values of TCS, 5-FU, and PG, for osteogenic differentiation ($ID_{50\ osteo}$) were calculated (Table S2).

3.4. Embryotoxicity prediction of TCS

As described previously (Cheng et al., 2016b; de Jong et al., 2014), the IC_{50} and ID_{50} values were substituted into the three EST prediction formulas to predict embryotoxicity.

The formulas were as follows:

$$I\ 5.916 \times \lg(IC_{50\ 3T3}) + 3.500 \times \lg(IC_{50\ ESC}) - 5.307 \times [(IC_{50\ 3T3} - ID_{50}) \div IC_{50\ 3T3}] - 15.27$$

$$II\ 3.651 \times \lg(IC_{50\ 3T3}) + 2.394 \times \lg(IC_{50\ ESC}) - 2.033 \times [(IC_{50\ 3T3} - ID_{50}) \div IC_{50\ 3T3}] - 6.85$$

$$III\ -0.125 \times \lg(IC_{50\ 3T3}) - 1.917 \times \lg(IC_{50\ ESC}) + 1.500 \times [(IC_{50\ 3T3} - ID_{50}) \div IC_{50\ 3T3}] - 2.67$$

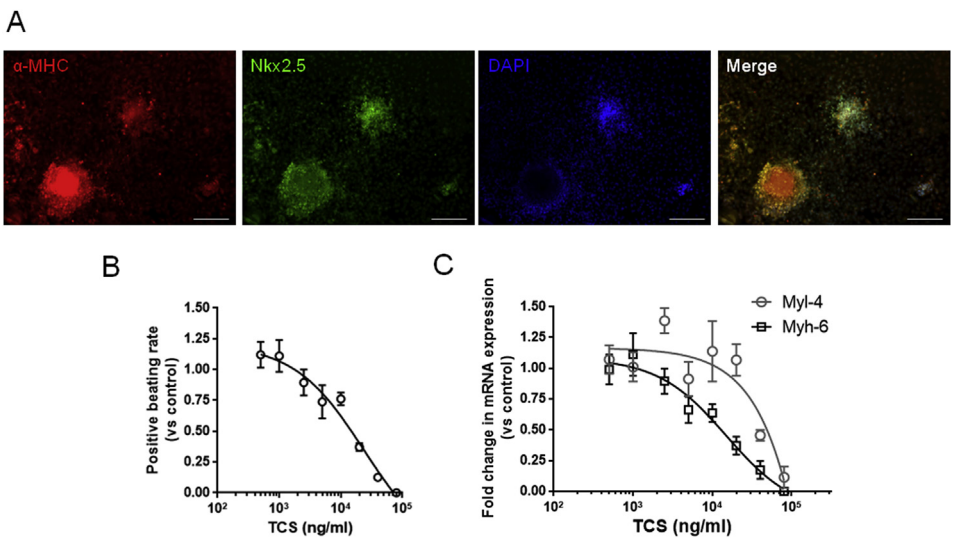

Fig. 2. TCS disrupted cardiac differentiation from ESCs. (A) Positive immunofluorescence staining of α-MHC and Nkx-2.5 in ESC-derived cardiomyocytes, indicating successful cardiac differentiation. Scale bar = 200 μm. (B) The change in positive beating rates of ESC-derived cardiomyocytes after exposure to 500–40,000 ng/ml TCS. N = 40 per concentration of TCS. (C) Relative mRNA expression of the cardiac-specific markers *Myh-6* and *Myl-4*, which were presented as dose-response curves to allow calculation of the $ID_{50\ cardio}$ value. The data from three independent experiments performed in triplicate are presented as the mean ± SEM. Scale bar = 200 μm.

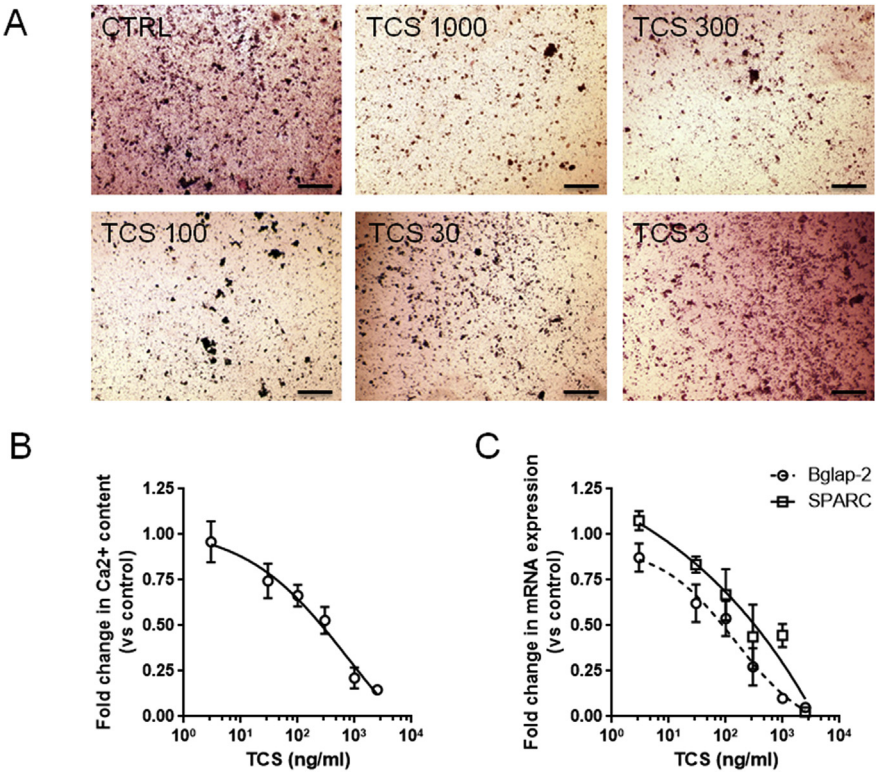

Fig. 3. TCS disrupted osteogenic differentiation from ESCs. (A) Results of ARS staining performed on Day 30 to evaluate the TCS-induced disruption in osteoblast differentiation. Scale bar = 100 μm. The cells were exposed to 3–2500 ng/ml TCS. (B) Relative calcium content compared with the control group. (C) Relative mRNA expression of *Bglap-2* and *SPARC* were presented as dose-response curves for $ID_{50\ osteo}$ value calculation. The data from three independent experiments performed in triplicate are presented as the mean ± SEM.

If I > II and I > III, the prediction result would be non-embryotoxic. If II > I and II > III, the prediction result would be weakly embryotoxic. If III > I and III > II, the prediction result would be strongly embryotoxic (Seiler and Spielmann, 2011); as the EST requires the input values in μg/ml, the data presented in Table 1 for EST prediction were re-presented.

The positive-control 5-FU was predicted as strongly embryotoxic, whereas the negative-control PG was evaluated as non-embryotoxic, both in EST_{cardio} and EST_{osteo} (Table S2), which matched the teratogenicity results of these chemicals *in vivo* and demonstrated the feasibility of EST for accurate embryotoxicity screening.

Therefore, TCS was predicted to be weakly embryotoxic in EST_{cardio}, but strongly embryotoxic in EST_{osteo}. First, the different prediction results suggested that TCS may discriminately disturb organogenesis. The process of osteogenesis, rather than cardiogenesis, may be more sensitive to the interference induced by TCS.

3.5. Low-dose TCS disrupted the osteogenic differentiation of ESC via the BMP-Smad signalling pathway

To further determine the potential mechanism of TCS-induced disruption, the BMP-Smad signalling pathway, which controlled the osteogenic differentiation of ESCs *in vitro*, was followed.

Upstream of the pathway, only in the 3 ng/ml TCS group, a significant increase in *BMP-2* and decrease in *Smad-4* mRNA expression were observed (Fig. 4A and B) compared with the control group. The mRNA expression of *Sp-7*, an osteogenic-specific transcription factor, was drastically upregulated by 300 ng/ml TCS (Fig. 4C). This alteration was accompanied by a significant inhibition on AKP activity (Fig. 4E) and a significant enhancement in TRAP activity (Fig. 4F), which suggested a trend in imbalanced differentiation toward osteoclasts was induced by high dosage of TCS only.

Another osteogenic-specific transcription factor, *Runx-2*, was inhibited by TCS, even at a low dosage (3 ng/ml) within the range of reported human internal exposure levels (0.01–38 ng/ml) (Philippat et al., 2013; Scinicariello and Buser, 2016; Wang et al., 2018), both transcriptionally and translationally (Fig. 4D and G).

To compare the toxic mechanisms of low-dose TCS, TX and E2 were selected as the negative- and positive-control, as the effect of these on the BMP-Smad signalling pathway has been well identified (Kolind et al., 2015; Yamamoto et al., 2002).

The protein levels of BMP-2 and the phosphorylation of Smad-1 were decreased by TX; and downstream, the protein levels of Runx-2 and Bglap-2 were also decreased (Fig. 5C–E), which caused a decrease in calcium content in ESC-derived osteoblasts (Fig. 5F and G), with no induction of cytotoxicity (Fig. S2) compared with the control group. In contrast, E2 upregulated the protein levels of BMP-2, Runx-2, and Bglap-2, by boosting the phosphorylation of Smad-1. Consequently, it resulted in a significant increase in calcium content, with no impairment on cellular viability compared with the control group (Fig. 5 and Fig. S2).

Low-dose TCS significantly decreased the phosphorylation of Smad-1 and inhibited the expression of Runx-2 and Bglap-2, as well as the calcification in ESC-derived osteoblasts (Fig. 5). The TCS + TX treatment did not decrease the phosphorylation of Smad-1, or the downstream Runx-2 and Bglap-2, but slightly decreased the calcium content in ESC-derived osteoblasts. Although the TCS + E2 treatment enhanced the phosphorylation of Smad-1, and increased the Bglap-2 level significantly, Runx-2 was still markedly inhibited (Fig. 5D). In addition, the calcium content was significantly lower than that in the control group (Fig. 5G).

These data provided preliminary evidence that TCS may play a specific role in the disruption of osteogenic-specific transcription factors.

3.6. Low-dose TCS interrupted the mitogen-activated protein kinase (MAPK) and BMP-Smad signalling pathway during osteogenic differentiation of ESCs

Based on to reduced phosphorylation of Smad-1 by low-dose TCS (Fig. 5C), and as that the MAPK signalling affects the phosphorylation and activation of Smad-1, the effect of low-dose TCS on MAPK

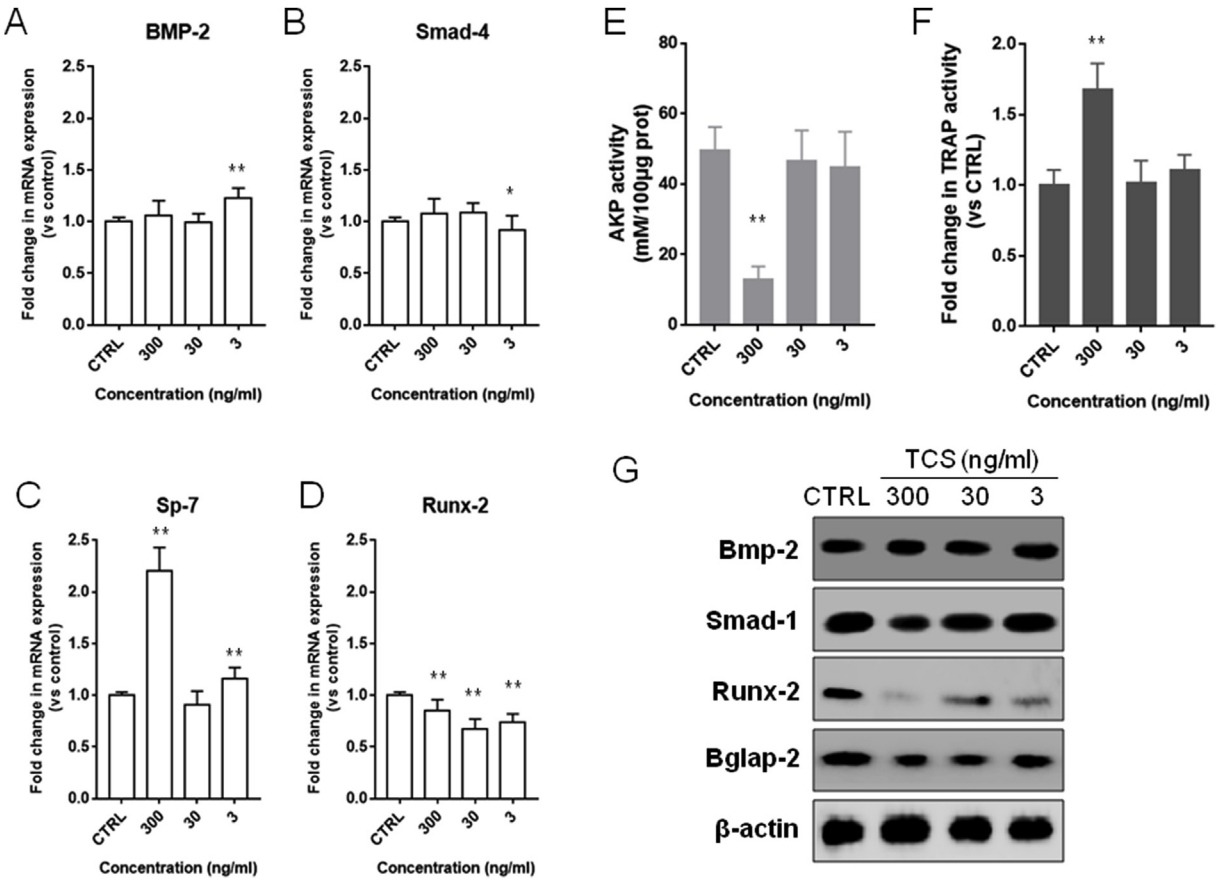

Fig. 4. TCS disturbed the Bmp-Smad signalling pathway during osteogenic differentiation of ESCs. (A) and (B) represented the changes in the mRNA expression of (A) *BMP-2*, (B) *Smad-4*, and their downstream osteogenic transcription factors (C) *Sp-7* and (D) *Runx-2* when cells were exposed to 3–1000 ng/ml TCS. (E) AKP activity and (F) TRAP activity were changed by 300 ng/ml of TCS only. The protein expression (G) of BMP-Smad signalling pathway and osteogenic markers altered by TCS was detected. The data from three independent experiments performed in triplicate are presented as the mean ± SEM. $*p < 0.05$, $**p < 0.0001$, compared with the control group.

signalling was investigated.

The positive control E2 increased the ratio of p-ERK/ERK and p-p38/p38 significantly, whereas the negative control TX decreased the ratio of p-ERK/ERK and p-JNK/JNK, but significantly increased the ratio of p-p38/p38 compared with the control group (Fig. 6). These changes agreed with those reported previously (Castillo et al., 2014; Thummuri et al., 2015). Low-dose TCS downregulated the ratio of p-ERK/ERK, but significantly increased the ratio of p-p38/p38, with no effect on JNK. Meanwhile, co-treatment with TCS and TX decreased the p-JNK/JNK ratio, but significantly enhanced the p-p38/p38 ratio, without any effect on p-ERK/ERK compared with the administration of TCS only. In contrast, TCS + E2 treatment led to no significant changes in p-ERK/ERK, p-JNK/JNK, or p-p38/p38 compared with the administration of TCS only. The treatments of TCS + TX and TCS + E2 resulted in a significant decrease in the phosphorylation of ERK compared with the control group, similar to that of TCS. The change was different to that observed in the TX or E2 groups, which supported that TCS induced a specific mechanism of ERK activation (Fig. 6).

Further, the inhibitory effect on ERK phosphorylation of TCS was referred to the ERK inhibitor FR180204. On Day 25 of the osteogenic differentiation of ESCs, the cells were treated with FR180204 (500 nM) and TCS (3 ng/ml) until Day 30. It was found that FR180204 inhibited the phosphorylation of Smad-1 and caused a significant decrease in the protein expression of Runx-2 and Bglap-2, with a tendency to inhibit Bglap-2 (Fig. 7A and B), and finally resulted in a reduction in the calcium content of ESC-derived osteoblasts (Fig. 7C). When cells were co-treated with TCS and FR180204, the phosphorylation of Smad-1 was significantly inhibited, together with severe inhibition of Runx-2 and Bglap-2 expression (Fig. 7A–D), with a tendency to inhibit Runx-2. In addition, the calcium content was decreased significantly (Fig. 7E and F) compared with the FR180204 group and the control group.

In summary, the mechanism of action of TCS on ERK phosphorylation was suggestive. Low-dose TCS affected ERK/BMP/Smad signalling, which caused a reduction in the expression of osteogenic-specific transcription factor Runx-2, and impaired calcification during osteogenic differentiation of ESCs *in vitro*.

4. Discussion

TCS has been utilized widely in personal care products or medical devices, such as sutures, owing to its antibacterial properties (Johnson et al., 2016). Even though the adverse effects of TCS on different organs have been studied for decades, the mechanism of toxicity is still not well understood, especially during the stages of embryo development.

Therefore, we first utilized a “dual-organ”-based EST to evaluate the embryotoxicity of TCS. The EST was developed by testing different classes of model chemicals for which background information on developmental toxicity was well known, and it could be used to predict and screen the embryotoxicity of chemicals into three embryotoxic classes, based on mathematical formulas with input values acquired from defined parameters (Chen et al., 2015a; Seiler and Spielmann, 2011). The IC_{50} values for NIH3T3 cells and ESCs, and the ID_{50} values of ESC differentiation to cardiomyocytes and osteoblasts, were obtained following chemical exposure. The molecular endpoints for ID_{50} determination, such as *Myh-6*, *Myl-4*, and *cTnT*, are essentially relevant to the contractile phenotype of cardiomyocytes derived from ESCs (Cheng

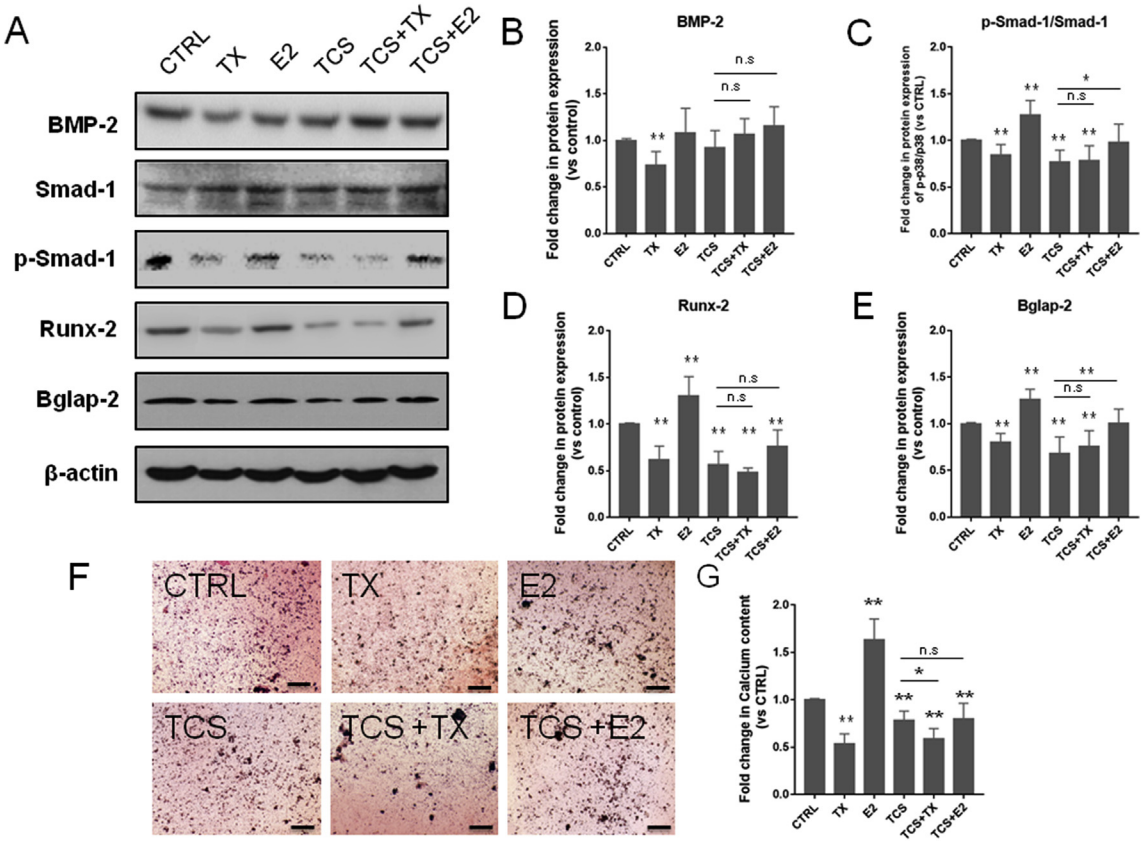

Fig. 5. Low-dose TCS-induced disruption in the BMP-Smad signalling pathway compared with tamoxifen (TX) and oestradiol (E2) during osteogenic differentiation from ESCs. (A) to (E) The western blotting bands of BMP-2, Smad-1, p-Smad-1, Runx-2, Bglap-2, and β-actin, as well as their quantitative expression in ESC-derived osteoblasts, respectively. (F) and (G) The calcium content of cells were exposed to TCS and TX or E2. Scale bar = 100 μm. The data from three independent experiments are presented as the mean ± SEM. $*p < 0.05$, $**p < 0.0001$, n.s. not significant compared with the control group.

et al., 2016b; Dimopoulou et al., 2018). Similarly, the molecular markers, such as *SPARC* and *Runx-2*, are important for the calcification phenotype of osteoblasts. The changes of these *in vitro* molecular markers have been validated to be highly correlated and concordant with the *in vivo* phenotype induced by various chemicals for which background information on developmental toxicity is well established (de Jong et al., 2014; zur Nieden et al., 2010).

In previous studies, increases in *Myl-4* and *Nkx-2.5* by PFOS for a hypoplastic cardiomyopathy phenotype (Cheng et al., 2013; Pashmforoush et al., 2004), and decreases in *Myh-6* with *Gata-4* by cigarette smoke extract *in vitro* with atrioventricular septal defect potential (Cheng et al., 2016a; Misra et al., 2014), were identified and investigated by the EST. Therefore, by utilizing the EST, not only the embryotoxicity of chemicals could be determined, but also the

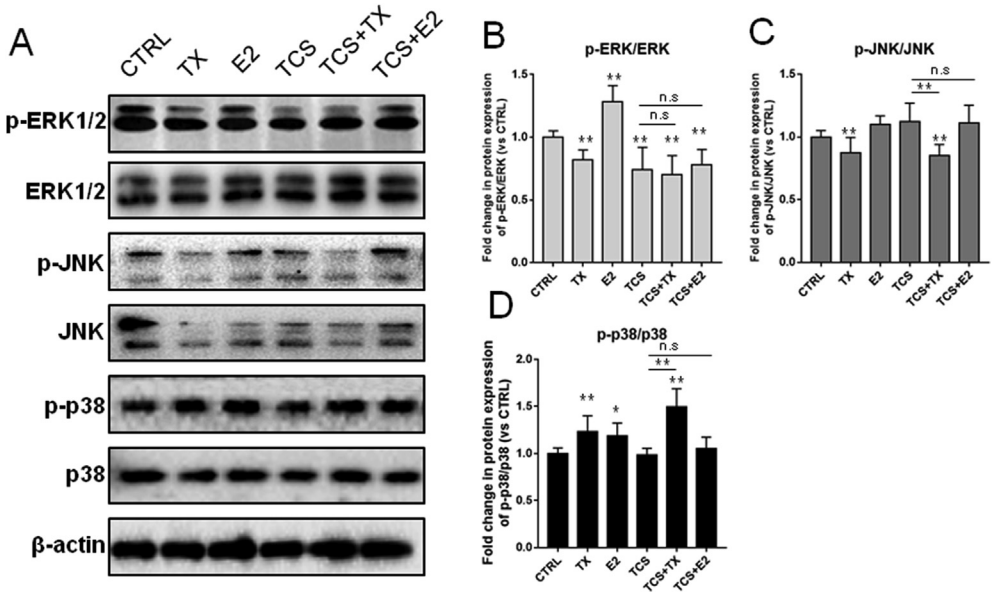

Fig. 6. The protein expression related to the MAPK pathway in ESC-derived osteoblasts following exposure to TCS and TX/E2. (A) to (D) The western blotting bands of total and phosphorylated ERK, JNK, and p38 normalized to β-actin and the quantitation. The data from three independent experiments are shown as the mean ± SEM. $*p < 0.05$, $**p < 0.0001$, n.s. not significant compared with the control group.

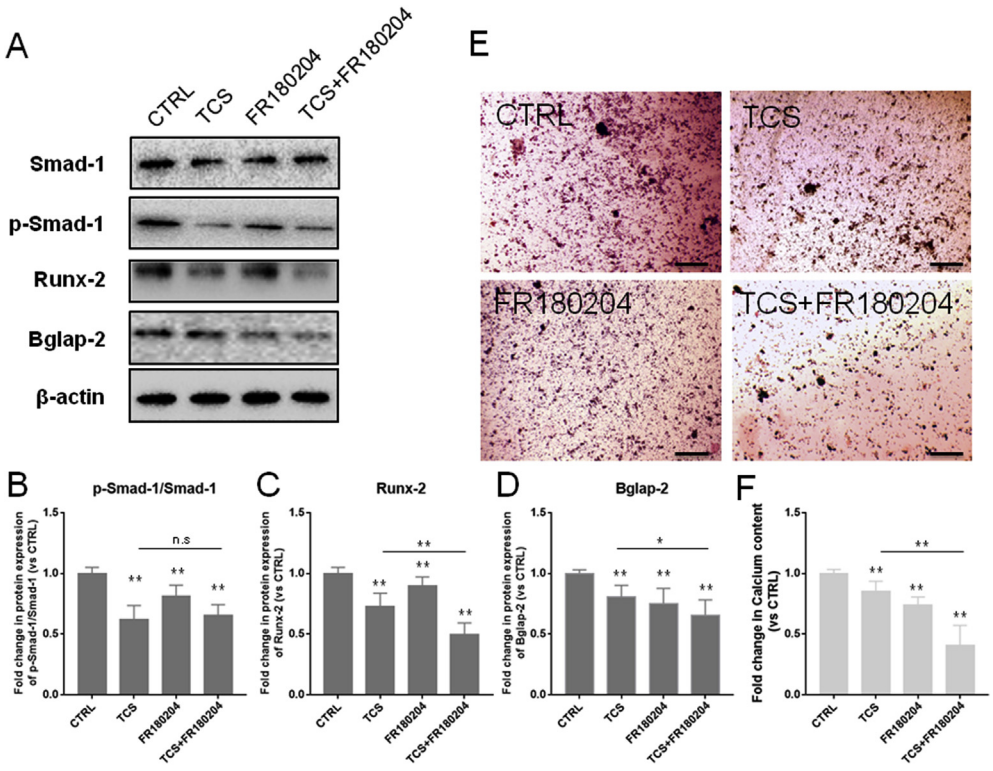

Fig. 7. Effect of ERK inhibitors on TCS-disrupted osteogenic differentiation in ESC-derived osteoblasts. (A) to (D) The western blotting bands of Smad-1, p-Smad-1, Runx-2, Bglap-2, and β-actin, as well as their quantitative expression, together with (E) ARS staining and (F) calcium content when cells were exposed to TCS and ERK inhibitor FR180204 in ESC-derived osteoblasts. Scale bar = 100 μm. The data from three independent experiments are presented as the mean ± SEM. $*p < 0.05$, $**p < 0.0001$, n.s. not significant compared with the control group.

teratogenicity potential, as well as the possible mechanisms of action of the chemicals. In addition, the involvement of an *in vitro* "multi-organ" test system would help to identify the target organ of chemicals, which would contribute to the improved power for hazard identification (Chen et al., 2015a; Lee et al., 2018).

Here, TCS was predicted to be weakly embryotoxic via EST_{cardio}, but was strongly embryotoxic via EST_{osteo}. This highlighted that TCS may induce adverse effects on the development of skeletal system specifically compared with that on the development of the heart.

In ESC-derived cardiomyocytes, changes in the positive beating rate and mRNA expression of *Myh-6* were coincident, whereas a higher expression of *Myl-4* was induced by low-dose TCS (Fig. 2C). Previously, it has been illustrated that the accumulation of *Myl-4* in diseased hearts, in the form of atrial to ventricular replacement, could be considered as a compensatory effect in response to the heart failure or hypertrophy of the left ventricle (Palmer, 2005), and to the congenital heart defect and cardiomyopathies involving pressure overload and tetralogy of Fallot (Morgenthau and Frishman, 2018). This indicates that the elevated expression of *Myl-4* during cardiogenesis after exposure to low-dose TCS (Fig. 2C) could not be considered as a sign of safety.

The development of skeletal system varies with developmental different stages, and there are many differences in foetal, neonatal, and adult bones with respect to metabolism and mineral homeostasis regulation (Kovacs, 2014, 2015). The osteoblasts originated from ESCs provide an ideal tool to study xenobiotic-induced adverse skeletal effects in a developmental perspective. Surprisingly, TCS produced obvious interference during osteogenesis, even at very low concentrations (Fig. 3). The ARS staining results visualized a dose-dependent decrease in the number and shape of calcified nodules in osteoblasts in response to TCS exposure. A more sensitive response to TCS was obtained from *Bglap-2* than *SPARC* (Fig. 3). The $ID_{50\ osteo}$ value was approximately 110 times lower than the value of $ID_{50\ cardio}$, which indicated that it was osteogenesis, rather than cardiogenesis, that specifically responded to TCS-induced disruption. This suggested that the skeletal system may be an underestimated target organ of TCS. Specifically, low-dose TCS was not cytotoxic to ESC-derived osteoblasts (Fig. 5A), although a remarkable reduction in calcium concentration was observed, even at a TCS dose as low as 3 ng/ml, which was within the range of human internal exposure levels previously reported (Philippat et al., 2013; Shekhar et al., 2017). The data provided preliminary evidence that TCS induced developmental toxicity in an osteogenic-specific way that was independent of its cytotoxicity.

The pluripotency maintenance of ESCs determines the possibility and fate of cells in terms of differentiation; thus, it is important to avoid any influence on the temporal and spatial expression of pluripotent markers (Haghverdi et al., 2015; Schwartz et al., 2015). It has been reported that among the pluripotent markers of ESC, only *Nanog* was affected by TCS at doses below 2.85 ng/ml (0.01 μmol/L). In contrast, significant changes in the expression of *Oct-4* and *Sox-2* were only observed at higher doses, and the AKP activity was not affected below 2895 ng/ml (10 μmol/L) TCS, which illustrated that pluripotency was impaired by high doses of TCS only (Chen et al., 2015b).

At the beginning of embryogenesis, upon binding to BMP ligands, the phosphorylated type-I receptor subsequently activates a set of Smads. The BMP-specific receptors regulate Smads, such as Smad-1/5/9, to form heteromeric complexes with a common-partner Smad, Smad-4, and translocate into the nucleus, where they regulate the transcription of various target genes, such as *Gata-4*, *Mef2c*, and *Nkx-2.5* during cardiogenesis, and further control their downstream transcripts *Myh-6* and *Myl-4* during heart development, to maintain the normal function and structure (Li et al., 2014; Morgenthau and Frishman, 2018; Vincentz et al., 2008). In addition, during the skeletal development, BMP-Smad signalling controls the transcription of *Sp-7* and *Runx-2,* and activates calcification, together with *Bglap-2*, in osteoblasts (Rashid et al., 2014; Salazar et al., 2016; Wu et al., 2016). Subsequently, osteoblasts express bone matrix protein genes at different levels depending on the maturation level of the cells. In mature osteoblasts, *Bglap-2* was strongly expressed, and a functional consequence of the *Runx-2/Sp-7* physical interaction has been identified by promoter-reporter assays (Rashid et al., 2014; Rendenbach et al., 2014). In *Runx-2*$^{-/-}$ mice, the expression of *Bglap-2* is virtually absent. In addition, *Runx-2* can upregulate the expression of bone matrix protein genes,

including *Col1a1*, *Spp1*, and *Bglap-2* (Komori, 2017; Qin et al., 2015). Collectively, the orchestration of *Sp-7*, *Runx-2*, and *Bglap-2* handles the precise regulation of osteogenesis *in vivo* and *in vitro*.

In the current study, remarkable inhibition of Runx-2 by TCS was observed at all doses (Fig. 4D and G), whereas a significant increase in Sp-7 by TCS was found at 300 ng/ml and 3 ng/ml TCS (Fig. 4C and D). The disproportionate effect on Sp-7 and Runx-2 induced by a non-cytotoxic dose of TCS, together with a decrease in calcification (Fig. 3A), indicated that Runx-2 was a potential target of TCS.

After consideration of the endocrine-disruptive property of TCS, TX and E2 were selected as negative and positive controls, respectively, to allow the effects on osteogenic differentiation to be compared (Berger et al., 2018; Hua et al., 2017; Wang et al., 2017a). (Ahn et al., 2008; Kammerer et al., 2013; Wang et al., 2018). Although the modes of action of TCS and TX on Runx-2 expression and calcification in ESC-derived osteoblasts were similar, TX impaired the BMP expression upstream, and hampered the signalling transduction, whereas TCS did not affect BMP. The reduced phosphorylation ratio of Smad-1 by TCS indicated that other signalling cascades handling the activation of phosphorylation may be involved.

The MAPK signalling pathway, which consists of a set of serine/threonine kinases, has been reported to play an important role in bone formation (Khatiwala et al., 2009). Through the evaluation of the protein expression of ERK, JNK, and p38, it was found that the function of ERK, rather than that of the JNK or p38, was specifically inhibited by low-dose TCS, with no recovery when cells were co-administered with TCS and E2 (Fig. 6). This finding agreed with a previous study (Park et al., 2016). It has been reported that ERK-mediated phosphorylation sites, such as S301, greatly affect the expression of Runx-2 (Artigas et al., 2014). In addition, ERK can bind to the promoter region of Bglap-2 to stimulate the osteogenic differentiation (Greenblatt et al., 2013; Wu et al., 2016). It was further confirmed in our study that the application of the ERK inhibitor FR180204 suppressed p-Smad-1, decreased the protein expression of both Runx-2 and Bglap-2, and resulted in a reduction of calcium content in ESC-derived osteoblasts (Fig. 7), which was similar to the mode of action of TX or TCS. However, it was notable that the co-administration of TCS and E2 returned the expression of Bglap-2 to that of the control group (Fig. 5E), but that Runx-2 was still significantly repressed (Fig. 5D) and accompanied by a decreased ratio of p-ERK/ERK (Fig. 6). These findings highlighted a sensitive and characteristic inhibition of Runx-2 via ERK/BMP/Smad signalling induced by TCS, even at a low dose, equivalent to human internal exposure.

The emerging concept of developmental origins of health and disease (DOHaD) emphasizes the connection between early-life exposure to xenobiotics and later-life disease (Haugen et al., 2015). As one of the risk factors, the effect of low-dose TCS on skeletal development may have been underestimated to date, and the potential risk to offspring should be of importance.

5. Conclusion

Low-dose TCS (3 ng/ml) interrupted the function of ERK/MAPK, regulated the BMP-Smad signalling pathway, and significantly reduced the expression of osteogenic markers Runx-2 and Bglap-2, which caused a decrease in the calcification of ESC-derived osteoblasts. The change induced in Runx-2 by low-dose TCS was different from the change in Bglap-2, and highlighted a specific target to monitor the adverse effects of TCS on skeletal development.

Conflicts of interest

The authors declare no conflict of interest.

Acknowledgements

This work was supported by the National Key R&D Program of China (2016YFC1000502), the National Natural Science Foundation of China (21577091), National key R&D program of China (2018YFC1602405), and the China Postdoctoral Science Foundation (2018M632143).

Appendix A. Supplementary data

Supplementary data to this article can be found online at https://doi.org/10.1016/j.fct.2019.02.038.

Transparency document

Transparency document related to this article can be found online at https://doi.org/10.1016/j.fct.2019.02.038.

References

Argus Research Laboratories Protocol number 403-010, A.R.L.P.n, 1992. Developmental Toxicity (Embryo-fetal Toxicity and Teratogenic Potential) Study of C-P Sample No. 38326 Administered Orally via the Diet to Crl:CD-1(ICR)BR Presumed Pregnant Mice. Sponsor's study number 92-001.

Ahn, K.C., Zhao, B., Chen, J., Cherednichenko, G., Sanmarti, E., Denison, M.S., Lasley, B., Pessah, I.N., Kultz, D., Chang, D.P., Gee, S.J., Hammock, B.D., 2008. In vitro biologic activities of the antimicrobials triclocarban, its analogs, and triclosan in bioassay screens: receptor-based bioassay screens. Environ. Health Perspect. 116, 1203–1210.

Artigas, N., Urena, C., Rodriguez-Carballo, E., Rosa, J.L., Ventura, F., 2014. Mitogen-activated protein kinase (MAPK)-regulated interactions between Osterix and Runx2 are critical for the transcriptional osteogenic program. J. Biol. Chem. 289, 27105–27117.

Axelstad, M., Boberg, J., Vinggaard, A.M., Christiansen, S., Hass, U., 2013. Triclosan exposure reduces thyroxine levels in pregnant and lactating rat dams and in directly exposed offspring. Food Chem. Toxicol. : an international journal published for the British Industrial Biological Research Association 59, 534–540.

Berger, K., Gunier, R.B., Chevrier, J., Calafat, A.M., Ye, X., Eskenazi, B., Harley, K.G., 2018. Associations of maternal exposure to triclosan, parabens, and other phenols with prenatal maternal and neonatal thyroid hormone levels. Environ. Res. 165, 379–386.

Castillo, A.B., Triplett, J.W., Pavalko, F.M., Turner, C.H., 2014. Estrogen receptor-beta regulates mechanical signalling in primary osteoblasts. Am. J. Physiol. Endocrinol. Metab. 306, E937–E944.

Chen, X., Hansen, D.K., Merry, G., DeJarnette, C., Nolen, G., Sloper, D., Fisher, J.E., Harrouk, W., Tassinari, M.S., Inselman, A.L., 2015a. Developing osteoblasts as an endpoint for the mouse embryonic stem cell test. Reprod. Toxicol. 53, 131–140.

Chen, X., Xu, B., Han, X., Mao, Z., Chen, M., Du, G., Talbot, P., Wang, X., Xia, Y., 2015b. The effects of triclosan on pluripotency factors and development of mouse embryonic stem cells and zebrafish. Arch. Toxicol. 89, 635–646.

Cheng, W., Yu, Z., Feng, L., Wang, Y., 2013. Perfluorooctane sulfonate (PFOS) induced embryotoxicity and disruption of cardiogenesis. Toxicol. Vitro : an international journal published in association with BIBRA 27, 1503–1512.

Cheng, W., Zhou, R., Feng, Y., Wang, Y., 2016a. Mainstream smoke and sidestream smoke affect the cardiac differentiation of mouse embryonic stem cells discriminately. Toxicology 357–358, 1–10.

Cheng, W., Zhou, R., Liang, F., Wei, H., Feng, Y., Wang, Y., 2016b. Application of mouse embryonic stem cell test to detect gender-specific effect of chemicals: a supplementary tool for embryotoxicity prediction. Chem. Res. Toxicol. 29, 1519–1533.

de Jong, E., van Beek, L., Piersma, A.H., 2014. Comparison of osteoblast and cardiomyocyte differentiation in the embryonic stem cell test for predicting embryotoxicity in vivo. Reprod. Toxicol. 48, 62–71.

Dimopoulou, M., Verhoef, A., Gomes, C.A., van Dongen, C.W., Rietjens, I., Piersma, A.H., van Ravenzwaay, B., 2018. A comparison of the embryonic stem cell test and whole embryo culture assay combined with the BeWo placental passage model for predicting the embryotoxicity of azoles. Toxicol. Lett. 286, 10–21.

Farmer, W.T., Louis, G.W., Buckalew, A.R., Hallinger, D.R., Stoker, T.E., 2018. Evaluation of triclosan in the Hershberger and H295R steroidogenesis assays. Toxicol. Lett. 291, 194–199.

Greenblatt, M.B., Shim, J.H., Glimcher, L.H., 2013. Mitogen-activated protein kinase pathways in osteoblasts. Annu. Rev. Cell Dev. Biol. 29, 63–79.

Haggard, D.E., Noyes, P.D., Waters, K.M., Tanguay, R.L., 2016. Phenotypically anchored transcriptome profiling of developmental exposure to the antimicrobial agent, triclosan, reveals hepatotoxicity in embryonic zebrafish. Toxicol. Appl. Pharmacol. 308, 32–45.

Haghverdi, L., Buettner, F., Theis, F.J., 2015. Diffusion maps for high-dimensional single-cell analysis of differentiation data. Bioinformatics 31, 2989–2998.

Haugen, A.C., Schug, T.T., Collman, G., Heindel, J.J., 2015. Evolution of DOHaD: the impact of environmental health sciences. Journal of developmental origins of health and disease 6, 55–64.

Ho, J.C.H., Hsiao, C.D., Kawakami, K., Tse, W.K.F., 2016. Triclosan (TCS) exposure

impairs lipid metabolism in zebrafish embryos. Aquat. Toxicol. 173, 29–35.
Hua, X., Cao, X.Y., Wang, X.L., Sun, P., Chen, L., 2017. Exposure of pregnant mice to triclosan causes insulin resistance via thyroxine reduction. Toxicol. Sci. : an official journal of the Society of Toxicology 160, 150–160.
Ibtisham, F., Nawab, A., Zhao, Y., 2016. Effect of antimicrobial triclosan on reproductive system of male rat. Pharm. Anal. Acta 7.
Jackson, E.N., Rowland-Faux, L., James, M.O., Wood, C.E., 2018. Administration of low dose triclosan to pregnant ewes results in placental uptake and reduced estradiol sulfotransferase activity in fetal liver and placenta. Toxicol. Lett. 294, 116–121.
Jain, R., Li, D., Gupta, M., Manderfield, L.J., Ifkovits, J.L., Wang, Q., Liu, F., Liu, Y., Poleshko, A., Padmanabhan, A., Raum, J.C., Li, L., Morrisey, E.E., Lu, M.M., Won, K.J., Epstein, J.A., 2015. HEART DEVELOPMENT. Integration of Bmp and Wnt signalling by Hopx specifies commitment of cardiomyoblasts. Science 348, aaa6071.
James, M.O., Li, W., Summerlot, D.P., Rowland-Faux, L., Wood, C.E., 2010. Triclosan is a potent inhibitor of estradiol and estrone sulfonation in sheep placenta. Environ. Int. 36, 942–949.
Johnson, P.I., Koustas, E., Vesterinen, H.M., Sutton, P., Atchley, D.S., Kim, A.N., Campbell, M., Donald, J.M., Sen, S., Bero, L., Zeise, L., Woodruff, T.J., 2016. Application of the Navigation Guide systematic review methodology to the evidence for developmental and reproductive toxicity of triclosan. Environ. Int. 92–93, 716–728.
Kamelia, L., Louisse, J., de Haan, L., Rietjens, I., Boogaard, P.J., 2017. Prenatal developmental toxicity testing of petroleum substances: application of the mouse embryonic stem cell test (EST) to compare in vitro potencies with potencies observed in vivo. Toxicol. Vitro : an international journal published in association with BIBRA 44, 303–312.
Kammerer, M., Gutzwiller, S., Stauffer, D., Delhon, I., Seltenmeyer, Y., Fournier, B., 2013. Estrogen Receptor alpha (ERalpha) and Estrogen Related Receptor alpha (ERRalpha) are both transcriptional regulators of the Runx2-I isoform. Mol. Cell. Endocrinol. 369, 150–160.
Khatiwala, C.B., Kim, P.D., Peyton, S.R., Putnam, A.J., 2009. ECM compliance regulates osteogenesis by influencing MAPK signalling downstream of RhoA and ROCK. J. Bone Miner. Res. : the official journal of the American Society for Bone and Mineral Research 24, 886–898.
Kolind, M., Bobyn, J.D., Matthews, B.G., Mikulec, K., Aiken, A., Little, D.G., Kalajzic, I., Schindeler, A., 2015. Lineage tracking of mesenchymal and endothelial progenitors in BMP-induced bone formation. Bone 81, 53–59.
Komori, T., 2017. Roles of Runx2 in skeletal development. Adv. Exp. Med. Biol. 962, 83–93.
Kovacs, C.S., 2014. Bone development and mineral homeostasis in the fetus and neonate: roles of the calciotropic and phosphotropic hormones. Physiol. Rev. 94, 1143–1218.
Kovacs, C.S., 2015. Calcium, phosphorus, and bone metabolism in the fetus and newborn. Early Hum. Dev. 91, 623–628.
Lee, J.H., Park, S.Y., Ahn, C., Kim, C.W., Kim, J.E., Jo, N.R., Kang, H.Y., Yoo, Y.M., Jung, E.M., Kim, E.M., Kim, K.S., Choi, K.C., Lee, S.D., Jeung, E.B., 2018. Pre-validation study of alternative developmental toxicity test using mouse embryonic stem cell-derived embryoid bodies. Food Chem. Toxicol. : An International Journal Published for the British Industrial Biological Research Association 123, 50–56.
Li, X., Martinez-Fernandez, A., Hartjes, K.A., Kocher, J.P., Olson, T.M., Terzic, A., Nelson, T.J., 2014. Transcriptional atlas of cardiogenesis maps congenital heart disease interactome. Physiol. Genom. 46, 482–495.
Misra, C., Chang, S.W., Basu, M., Huang, N., Garg, V., 2014. Disruption of myocardial Gata4 and Tbx5 results in defects in cardiomyocyte proliferation and atrioventricular septation. Hum. Mol. Genet. 23, 5025–5035.
Morgenthau, A., Frishman, W.H., 2018. Genetic origins of tetralogy of fallot. Cardiol. Rev. 26, 86–92.
Palmer, B.M., 2005. Thick filament proteins and performance in human heart failure. Heart Fail. Rev. 10, 187–197.
Park, B.K., Gonzales, E.L., Yang, S.M., Bang, M., Choi, C.S., Shin, C.Y., 2016. Effects of triclosan on neural stem cell viability and survival. Biomolecules & therapeutics 24, 99–107.
Pashmforoush, M., Lu, J.T., Chen, H., Amand, T.S., Kondo, R., Pradervand, S., Evans, S.M., Clark, B., Feramisco, J.R., Giles, W., Ho, S.Y., Benson, D.W., Silberbach, M., Shou, W., Chien, K.R., 2004. Nkx2-5 pathways and congenital heart disease; loss of ventricular myocyte lineage specification leads to progressive cardiomyopathy and complete heart block. Cell 117, 373–386.
Pernoncini, K.V., Montagnini, B.G., de Goes, M.L.M., Garcia, P.C., Gerardin, D.C.C., 2018. Evaluation of reproductive toxicity in rats treated with triclosan. Reprod. Toxicol. 75, 65–72.
Philippat, C., Wolff, M.S., Calafat, A.M., Ye, X., Bausell, R., Meadows, M., Stone, J., Slama, R., Engel, S.M., 2013. Prenatal exposure to environmental phenols: concentrations in amniotic fluid and variability in urinary concentrations during pregnancy. Environ. Health Perspect. 121, 1225–1231.
Qi, X., Yang, G., Yang, L., Lan, Y., Weng, T., Wang, J., Wu, Z., Xu, J., Gao, X., Yang, X., 2007. Essential role of Smad 4 in maintaining cardiomyocyte proliferation during murine embryonic heart development. Dev. Biol. 311, 136–146.
Qin, X., Jiang, Q., Matsuo, Y., Kawane, T., Komori, H., Moriishi, T., Taniuchi, I., Ito, K., Kawai, Y., Rokutanda, S., Izumi, S., Komori, T., 2015. Cbfb regulates bone development by stabilizing Runx family proteins. J. Bone Miner. Res. : the official journal of the American Society for Bone and Mineral Research 30, 706–714.
Rashid, H., Ma, C., Chen, H., Wang, H., Hassan, M.Q., Sinha, K., de Crombrugghe, B., Javed, A., 2014. Sp7 and Runx2 molecular complex synergistically regulate expression of target genes. Connect. Tissue Res. 55 (Suppl. 1), 83–87.
Rendenbach, C., Yorgan, T.A., Heckt, T., Otto, B., Baldauf, C., Jeschke, A., Streichert, T., David, J.P., Amling, M., Schinke, T., 2014. Effects of extracellular phosphate on gene expression in murine osteoblasts. Calcif. Tissue Int. 94, 474–483.
Rodricks, J.V., Swenberg, J.A., Borzelleca, J.F., Maronpot, R.R., Shipp, A.M., 2010. Triclosan: a critical review of the experimental data and development of margins of safety for consumer products. Crit. Rev. Toxicol. 40, 422–484.
Salazar, V.S., Gamer, L.W., Rosen, V., 2016. BMP signalling in skeletal development, disease and repair. Nat. Rev. Endocrinol. 12, 203–221.
Saley, A., Hess, M., Miller, K., Howard, D., King-Heiden, T.C., 2016. Cardiac toxicity of triclosan in developing zebrafish. Zebrafish 13, 399–404.
Schwartz, M.P., Hou, Z., Propson, N.E., Zhang, J., Engstrom, C.J., Santos Costa, V., Jiang, P., Nguyen, B.K., Bolin, J.M., Daly, W., Wang, Y., Stewart, R., Page, C.D., Murphy, W.L., Thomson, J.A., 2015. Human pluripotent stem cell-derived neural constructs for predicting neural toxicity. Proc. Natl. Acad. Sci. U.S.A. 112, 12516–12521.
Scinicariello, F., Buser, M.C., 2016. Serum testosterone concentrations and urinary bisphenol A, benzophenone-3, triclosan, and paraben levels in male and female children and adolescents: NHANES 2011-2012. Environ. Health Perspect. 124, 1898–1904.
Seiler, A.E., Spielmann, H., 2011. The validated embryonic stem cell test to predict embryotoxicity in vitro. Nat. Protoc. 6, 961–978.
Shekhar, S., Sood, S., Showkat, S., Lite, C., Chandrasekhar, A., Vairamani, M., Barathi, S., Santosh, W., 2017. Detection of phenolic endocrine disrupting chemicals (EDCs) from maternal blood plasma and amniotic fluid in Indian population. Gen. Comp. Endocrinol. 241, 100–107.
Shi, G., Cui, Q., Pan, Y., Sheng, N., Sun, S., Guo, Y., Dai, J., 2017. 6:2 Chlorinated polyfluorinated ether sulfonate, a PFOS alternative, induces embryotoxicity and disrupts cardiac development in zebrafish embryos. Aquat. Toxicol. 185, 67–75.
Thummuri, D., Jeengar, M.K., Shrivastava, S., Nemani, H., Ramavat, R.N., Chaudhari, P., Naidu, V.G., 2015. Thymoquinone prevents RANKL-induced osteoclastogenesis activation and osteolysis in an in vivo model of inflammation by suppressing NF-KB and MAPK Signalling. Pharmacol. Res. 99, 63–73.
Vincentz, J.W., Barnes, R.M., Firulli, B.A., Conway, S.J., Firulli, A.B., 2008. Cooperative Interaction of Nkx2.5 and Mef2c Transcription Factors during Heart Development, vol. 237. Developmental dynamics : an official publication of the American Association of Anatomists, pp. 3809–3819.
Wang, C., Chen, L., Zhao, S., Hu, Y., Zhou, Y., Gao, Y., Wang, W., Zhang, J., Tian, Y., 2018. Impacts of prenatal triclosan exposure on fetal reproductive hormones and its potential mechanism. Environ. Int. 111, 279–286.
Wang, F., Guo, X., Chen, W., Sun, Y., Fan, C., 2017a. Effects of triclosan on hormones and reproductive axis in female Yellow River carp (Cyprinus carpio): potential mechanisms underlying estrogen effect. Toxicol. Appl. Pharmacol. 336, 49–54.
Wang, Z., Li, X., Klaunig, J.E., 2017b. Investigation of the mechanism of triclosan induced mouse liver tumors. Regul. Toxicol. Pharmacol. : RTP (Regul. Toxicol. Pharmacol.) 86, 137–147.
Wu, M., Chen, G., Li, Y.P., 2016. TGF-beta and BMP signalling in osteoblast, skeletal development, and bone formation, homeostasis and disease. Bone research 4, 16009.
Yamamoto, T., Saatcioglu, F., Matsuda, T., 2002. Cross-talk between bone morphogenic proteins and estrogen receptor signalling. Endocrinology 143, 2635–2642.
Yao, L., Zhao, J.L., Liu, Y.S., Zhang, Q.Q., Jiang, Y.X., Liu, S., Liu, W.R., Yang, Y.Y., Ying, G.G., 2018. Personal care products in wild fish in two main Chinese rivers: bioaccumulation potential and human health risks. Sci. Total Environ. 621, 1093–1102.
Yin, N., Liang, S., Liang, S., Yang, R., Hu, B., Qin, Z., Liu, A., Faiola, F., 2018. TBBPA and its alternatives disturb the early stages of neural development by interfering with the NOTCH and WNT pathways. Environ. Sci. Technol. 52, 5459–5468.
Yu, R., Miyamura, N., Okamoto-Uchida, Y., Arima, N., Ishigami-Yuasa, M., Kagechika, H., Nishina, H., 2015. A modified murine embryonic stem cell test for evaluating the teratogenic effects of drugs on early embryogenesis. PLoS One 10, e0145286.
zur Nieden, N.I., Davis, L.A., Rancourt, D.E., 2010. Monolayer cultivation of osteoprogenitors shortens duration of the embryonic stem cell test while reliably predicting developmental osteotoxicity. Toxicology 277, 66–73.
zur Nieden, N.I., Turgman, C.C., Lang, X., Larsen, J.M., Granelli, J., Hwang, Y.J., Lyubovitsky, J.G., 2015. Fluorescent hydrogels for embryoid body formation and osteogenic differentiation of embryonic stem cells. ACS Appl. Mater. Interfaces 7, 10599–10605.